THE UNIVERSITY of EDINBURGH

Edinburgh Research Explorer

First characterization of the SPADnet sensor

Citation for published version:
Gros-daillon, E, Maingault, L, André, L, Reboud, V, Verger, L, Charbon, E, Bruschini, C, Veerappan, C, Stoppa, D, Massari, N, Perenzoni, M, Braga, LHC, Gasparini, L, Henderson, RK, Walker, R, East, S, Grant, L, Jatekos, B, Lorincz, E, Ujhelyi, F, Erdei, G, Major, P, Papp, Z & Nemeth, G 2013, 'First characterization of the SPADnet sensor: a digital silicon photomultiplier for PET applications', *Journal of Instrumentation*, vol. 8, no. 12, pp. C12026-C12026. https://doi.org/10.1088/1748-0221/8/12/C12026

Digital Object Identifier (DOI):
10.1088/1748-0221/8/12/C12026

Link:
Link to publication record in Edinburgh Research Explorer

Published In:
Journal of Instrumentation

General rights
Copyright for the publications made accessible via the Edinburgh Research Explorer is retained by the author(s) and / or other copyright owners and it is a condition of accessing these publications that users recognise and abide by the legal requirements associated with these rights.

Take down policy
The University of Edinburgh has made every reasonable effort to ensure that Edinburgh Research Explorer content complies with UK legislation. If you believe that the public display of this file breaches copyright please contact openaccess@ed.ac.uk providing details, and we will remove access to the work immediately and investigate your claim.

OPEN ACCESS

Download date: 05. May. 2023

IOPscience iopscience.iop.org

Home Search Collections Journals About Contact us My IOPscience

First characterization of the SPADnet sensor: a digital silicon photomultiplier for PET applications

This content has been downloaded from IOPscience. Please scroll down to see the full text.

2013 JINST 8 C12026

(http://iopscience.iop.org/1748-0221/8/12/C12026)

View the table of contents for this issue, or go to the journal homepage for more

Download details:

IP Address: 129.215.183.211
This content was downloaded on 18/02/2015 at 10:12

Please note that terms and conditions apply.

PUBLISHED BY IOP PUBLISHING FOR SISSA MEDIALAB

RECEIVED: *October 1, 2013*
ACCEPTED: *December 3, 2013*
PUBLISHED: *December 19, 2013*

15th INTERNATIONAL WORKSHOP ON RADIATION IMAGING DETECTORS
23–27 JUNE 2013,
PARIS, FRANCE

2013 JINST 8 C12026

First characterization of the SPADnet sensor: a digital silicon photomultiplier for PET applications

E. Gros-Daillon,[a,1] **L. Maingault,**[a] **L. André,**[a] **V. Reboud,**[a] **L. Verger,**[a] **E. Charbon,**[b] **C. Bruschini,**[c] **C. Veerappan,**[b] **D. Stoppa,**[d] **N. Massari,**[d] **M. Perenzoni,**[d] **L.H.C. Braga,**[d] **L. Gasparini,**[d] **R.K. Henderson,**[e] **R. Walker,**[e] **S. East,**[f] **L. Grant,**[f] **B. Jatekos,**[g] **E. Lorincz,**[g] **F. Ujhelyi,**[g] **G. Erdei,**[g] **P. Major,**[h] **Z. Papp**[h] **and G. Nemeth**[h]

[a] *CEA-Leti, MINATEC Campus, Recherche Technologique, F 38054 Grenoble, France*
[b] *Delft University of Technology, Delft, The Netherlands*
[c] *École Polytechnique Fédérale de Lausanne, Lausanne, Switzerland*
[d] *Smart Optical Sensors and Interfaces (SOI) Group, Fondazione Bruno Kessler (FBK), Trento, Italy*
[e] *CMOS Sensors and Systems (CSS) Group, School of Engineering, The University of Edinburgh, Edinburgh, U.K.*
[f] *Imaging Division, STMicroelectronics, Edinburgh, U.K.*
[g] *Budapest University of Technology and Economics, Department of Atomic Physics, Budapest, Hungary*
[h] *Mediso Orvosi Berendezes Fejleszto es Szerviz Kft. (Mediso Ltd.), Budapest, Hungary*

E-mail: eric.grosdaillon@cea.fr

ABSTRACT: Silicon Photomultipliers have the ability to replace photomultiplier tubes when used as light sensors in scintillation gamma-ray detectors. Their timing properties, compactness, and magnetic field compatibility make them interesting for use in Time-of-Flight Magnetic Resonance Imaging compatible Positron Emission Tomography. In this paper, we present a new fully digital Single Photon Avalanche Diode (SPAD) based detector fabricated in CMOS image sensor technology. It contains 16x8 pixels with a pitch of 610x571.2 μm^2.

[1] Corresponding author.

© 2013 IOP Publishing Ltd and Sissa Medialab srl
doi:10.1088/1748-0221/8/12/C12026

The Dark Count Rate and the Photon Detection Probability of each SPAD has been measured and the homogeneity of these parameters in the entire 92000 SPAD array is shown. The sensor has been optically coupled to a single LYSO needle and a LYSO array. The scintillator crystal was irradiated with several gamma sources and the resulting images and energy spectra are presented.

KEYWORDS: Gamma detectors (scintillators, CZT, HPG, HgI etc); Photon detectors for UV, visible and IR photons (solid-state); Gamma camera, SPECT, PET PET/CT, coronary CT angiography (CTA)

2013 JINST 8 C12026

Contents

2013 JINST 8 C12026

1 Introduction

Current developments for Positron Emission Tomography follow two axes: The measurement of the gamma photons Time of Flight (ToF-PET) which improves the marker position determination, and the coupling of PET with a Magnetic Resonance Imaging scanner (PET-MRI) which provides soft-tissue contrast without the patient dose induced by Computed Tomography scanners. Silicon Photomultipliers (SiPM) are insensitive to the strong magnetic field of the MRI and are candidates to replace PhotoMultipliers Tubes (PMTs) for MRI compatible PET. Keeping the same performances as PMTs in term of counting photon and timing performance, the system electronic is simplified because a lot of support electronic is in the same silicon chip as the sensor.

Conventional SiPMs are currently commercially available and are widely studied, in particular for PET applications. In these devices, the SPADs are grouped in array to form pixels, and the outputs current are summed. Using CMOS technology, the digital SiPM concept, where each SPAD is individually digitized, has been proposed [1, 2]. Noisy SPADs could be disabled and timing information is generated on-chip. Recently, Multi time channel Digital SiPM (MD-SiPM) has been proposed [3], where several photon could be time stamped, potentially enabling a more robust timing resolution [4, 5].

In this paper, we present a new MD-SiPM for ToF-PET, compatible with computed tomography (CT) and MRI. The sensor architecture is described in section 2. The measurements set-ups are detailed in section 3 and the sensor characterization is presented in section 4. Finally, section 5 gives the conclusion.

2 Sensor description

The SPADnet sensor architecture and the SPADs implementation are fully described in ref. [6] and [7]. The main features are the following:

- The chip contains 16×8 pixels, each of them measures 0.610×0.571mm^2. This dimension is smaller than the PET spatial resolution, in order to compute a point of interaction using a slab scintillator [8, 9]. Each pixel contains a Time to Digital Converter (TDC): several photon timestamps are measured for each scintillation, in order to provide a robust timing resolution [4, 5].
- The SPADs have a circular shape and are organized in a honeycomb-like array with well sharing [10], meaning that their cathodes are shared, in order to improve the Fill Factor (FF). In order to be tolerant to noisy SPADs, each SPAD could be individually disabled using a programmable memory.
- In order to reduce the required electronic, therefore improving the SPAD fill factor, the information is compressed in space and time using the mini-SiPM concept [11], taking advantage of the relatively low photon flux. Each pixel contains four mini-SiPM composed by 180 SPADs and their respective front end together with the compression circuit.
- All fired SPADs across the whole chip are summed every 10ns. This discrete photon flux is compared to a threshold to determine when an event occurred, which triggers the integration.
- Chips are not wire bonded to a printed circuit board but benefit from the Through Silicon Via (TSV) technology. They could be tiled with very little space lost between chips. The used technology for the TSV realization implies the presence of a 500μm handling glass above the chip.

An evaluation kit, based on a SP605 board from Xilinx enables to plug easily the chip under test and is linked by an Ethernet cable to a computer. For each gamma event, the number of counts per pixel during the integration period, the TDC value of each pixel, and a time histogram containing the number of count at 100 MS/s are generated and could be processed using LabVIEW.

3 Electro-optical measurements

By using the memory programming, one SPAD per pixel could be select at a time. The Dark Count Rate (DCR) and the Photon Detection Probability (PDP) of each SPAD of the die, that is to say every 92K SPAD could be measured without any cross talk contribution. All measurements were made with an excess bias of 1.5V (which is a trade-off between PDP and DCR) and at room temperature.

3.1 Dark Count Rate

A typical DCR map with the associated dark count rate cumulative probability is shown in figure 1. The median DCR is 5kHz and the mean DCR is 24kHz. Putting this set-up in a temperature chamber, we have measured that the median DCR doubles every 17 °C and that the DCR probability remains homothetic as can be seen in figure 1 right.

2013 JINST 8 C12026

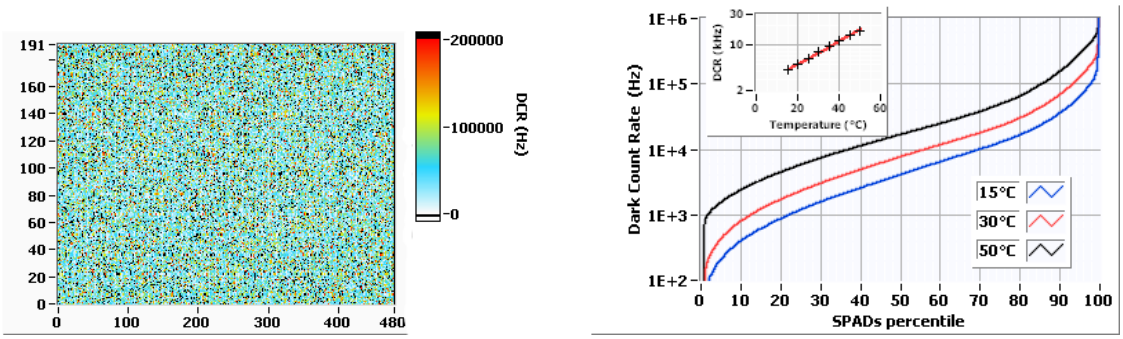

Figure 1. *Left:* typical DCR map at 35 ° C. *Right:* DCR cumulative probability with respect to temperature. Inset: median DCR with respect to temperature.

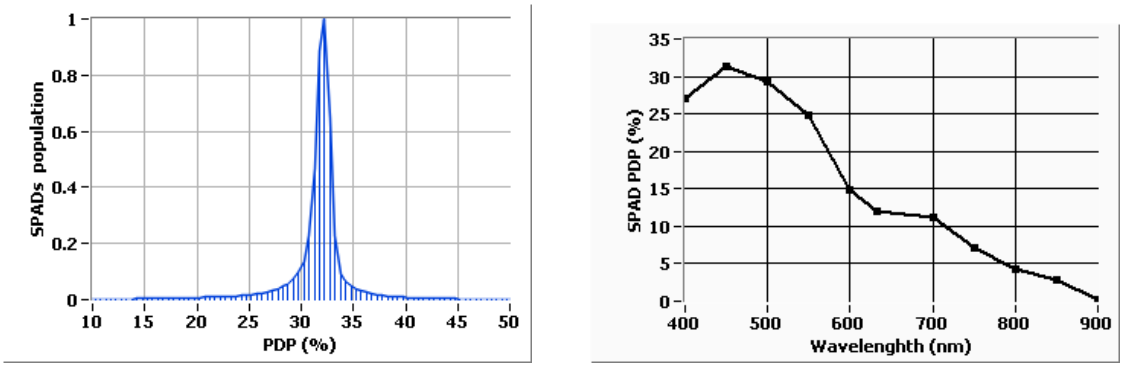

Figure 2. Normalized PDP distribution (left) and PDP with respect to wavelength (right).

3.2 Photon Detection Probability

In order to evaluate the SPADs PDP, a white light source whose wavelength is selected using a band pass filter (from 400nm to 900nm, 50 nm step, 10 nm-bandwidth) was used. Then a diffuser homogenizes the light which is then guided through a 1.50m-long black pipe to create a homogeneous distribution of parallel light on sensor axis. The incoming light is measured using a calibrated diode. The SPADs PDP is homogeneous (FWHM = 3%) as can be seen in figure 2 and peaks at 31% at 450nm (figure 2 right). To obtain the chip PDP, this number must be multiplied by the SPAD fill factor which is 42.6%, leading to a peak chip PDP at 13% at 450nm.

4 Gamma irradiation

A single LYSO scintillator crystal ($3.5\times3.5\times20$ mm^3) and a LYSO needles array (of 1.3x1.3x13mm^3 needles) which have respectively the typical dimension for clinical and preclinical imaging have been optically coupled to the SPADnet chip as depicted figure 3. For preclinical imaging, the crystal is thinner in order to reduce the parallax error due to the smaller ring radius. The sensor active area is 9.8×4.6mm^2. No particular alignment was performed between LYSO crystals and chips' pixels.

4.1 Using a single crystal

A LYSO scintillator crystal of $3.5\times3.5\times20$mm^3 from Saint Gobain, wrapped with Teflon was optically coupled to 9.8×4.6 mm^2 sensor active area using optical grease. A picture of the crystal

2013 JINST 8 C12026

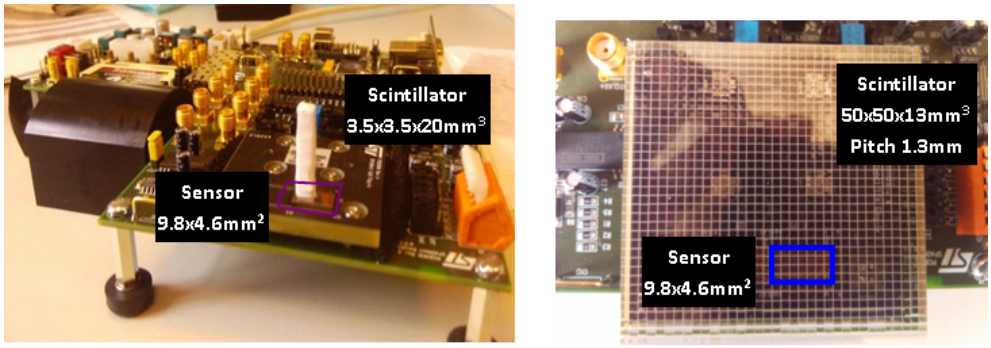

Figure 3. Pictures of the device under test. *Left:* single crystal needle. *Right:* array of LYSO crystals.

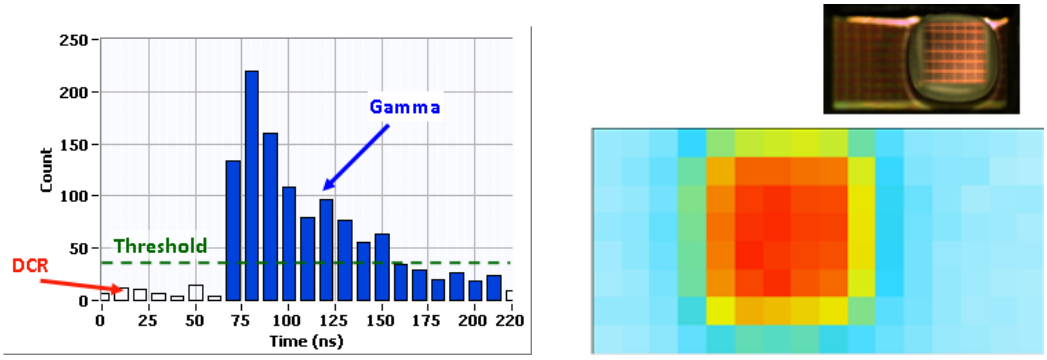

Figure 4. *Left:* digitized photon flux at 100MS/s consecutive to a gamma photon absorption. *Right:* accumulated gamma count. Inset: picture of the crystal before Teflon wrapping on the chip. Note that the crystal position has changed between the two images during to the Teflon wrapping operation.

(before Teflon wrapping) on the chip is shown on the figure 4 inset. For these measurements, the 20% noisier SPADs, with DCR above 20kHz, were disabled. Four gamma sources were placed above the crystal to probe different gamma photon energies: ^{241}Am (mainly 59.5keV, 1MBq), ^{57}Co (mainly 122keV, 2MBq), ^{133}Ba (mainly 80keV and 356keV, 1MBq) and ^{22}Na (511keV and 1275keV, 1MBq).

The figure 4 shows a typical digitized photon flux at 100MS/s, consecutive to a 511keV gamma photon absorption. Due to the system architecture, DCR does not affect the triggering system. The integration time, depicted in blue in the figure, was set to 150ns. The average image of these events enables to see a crystal (figure 4, right) slightly larger than the six pixels per side (36 pixels for the surface) directly under the LYSO crystal due to the 500μm thick glass attached on the chip for the TSV process. The crystal position is not the same as on the photography because the crystal was moved during the wrapping step.

The gamma spectrum obtained with the four gamma sources is plotted figure 5. The LYSO self-emission is also visible. Due to 176 Lutetium isotope, two gamma are emitted in coincidence, at 307keV and 202keV. If they are both absorbed by the crystal, a 509keV energy is detected. The main peaks of each gamma sources are resolved, from 59.5keV for the ^{241}Am source to 1275 keV for the ^{22}Na source. Due to the emitted photon statistic, the energy resolution improves from 40% FWHM at 59.5 keV to 13% FWHM at 511keV. A 54keV X-ray could escape from the LYSO crystal after a photoelectric interaction, resulting in a secondary peaks at lower energy than the

2013 JINST 8 C12026

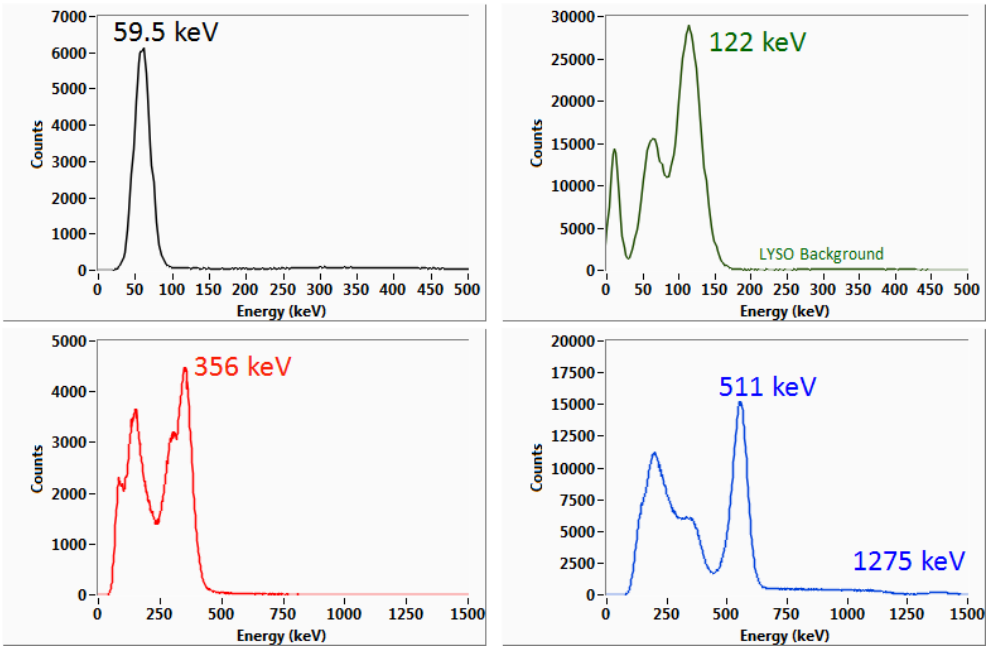

Figure 5. Gamma spectrum obtained with an Americium 241 source (black), a Cobalt 57 source (green), a Barium 133 source (red), and a Sodium 22 source (blue).

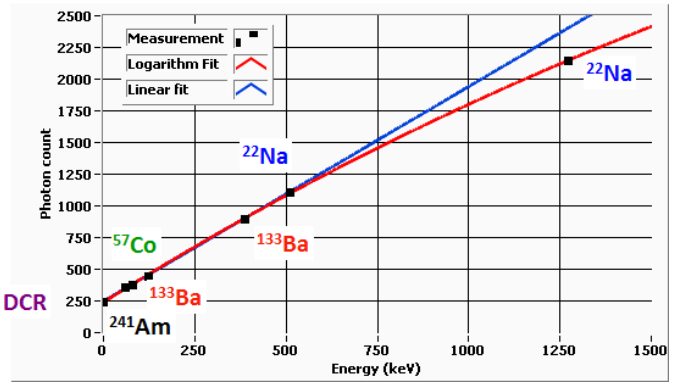

Figure 6. Number of counts with respect to the incident photon energy.

photoelectric peak. This escape peak is visible on the Cobalt and the Barium spectra, and is mixed with the photoelectric peak on the Sodium spectrum, worsening the energy resolution.

Each SPAD has a dead time of the order of the scintillation decay time, thus can only fire one time per gamma photon. Mainly due to the limited number of SPADs, and slightly to spatial and temporal compression, the number of counts with respect to the incident photon flux is sub-linear. The number of count with respect to the expected energy is plotted figure 6. For this configuration, the non-linearity at 511keV is below 1%.

4.2 Using a crystal array

In order to evaluate the sensor ability for preclinical imaging, a 13 mm thick LYSO array with 35×35 pixels, 1.3mm pitch, and optical separator, was coupled on the 9.8×4.6mm^2 active area

2013 JINST 8 C12026

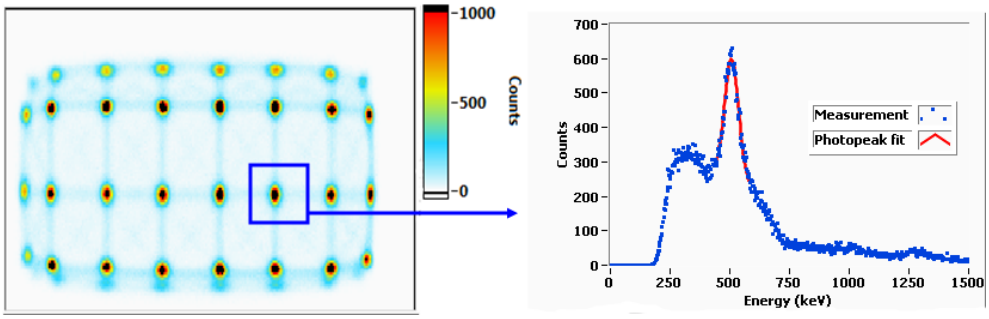

Figure 7. *Left:* image of scintillations. *Right:* energy spectrum from one single needle.

using optical grease. The crystal is thinner that for the clinical application in order to limit the parallax error due to the smaller diameter ring. There was no alignment of the LYSO needles with the sensor pixels. GORE Diffuse Reflector was deposit on the crystal backside to reflect the photons. The experimental set-up is pictured figure 3.

In order to determine each scintillation position, a software post processing was applied to each image: the noise was filtered, with a threshold fixed to 5 counts, and then a simple centre of gravity was computed. The LYSO needles are clearly resolved as can be seen in figure 7, except for the needles overflowing the chip. For this image, no energy windowing was used. The energy spectrum associated to a single needle is shown figure 7 right: the energy resolution at 511keV is 13% FWHM. The energy spectrum of the other needles is equivalent.

5 Conclusion

A Multi time channel Digital SiPM (MD-SiPM) for TOF-PET application, compatible with IRM was characterized. SPADnet is a 4-sided tileable gamma sensor in CMOS technology. It contains 8x16 pixels, 0.6 mm pitch, each of them embedding a Time to Digital Converter. The median Dark Count Rate at room temperature is 5kHz and the chip Photon Detection Probability peaks at 13% at 420nm. The energy resolution at 511keV was 13% FWHM with a 3.5×3.5×20mm LYSO crystal needle and 13% FWHM with an array of 1.3×1.3×13mm LYSO needles. Coincidence measurements with two sensors are ongoing.

In a close future, we will mount optical concentrators to recover SPADs fill factor loss, and tile the chips to build PET 50×50 mm detector modules which will be integrated into a PET ring.

Acknowledgments

This work, conceived within the SPADnet project (www.spadnet.eu), has been supported by the European Community within the Seventh Framework Programme ICT Photonics.

References

[1] T. Frach et al., *The digital silicon photomultiplier — Principle of operation and intrinsic detector performance*, *IEEE Nucl. Sci. Symp. Conf. Rec.* (2009) 2383.

2013 JINST 8 C12026

[2] C. Degenhardt et al., *The digital silicon photomultiplier — A novel sensor for the detection of scintillation light, IEEE Nucl. Sci. Symp. Conf. Rec.* (2009) 2383 .

[3] S. Mandai and E. Charbon, *Multi-channel digital SiPMs: concept, analysis and implementation*, *IEEE Nucl. Sci. Symp. Conf. Rec.* (2012) 1840.

[4] L.H.C. Braga et al., *A time of arrival estimator based on multiple timestamps for digital PET detectors*, *IEEE Nucl. Sci. Symp. Conf. Rec.* (2012) 1082.

[5] S. Seifert et al., *The lower bound on the timing resolution of scintillation detectors*, *Phys. Med. Biol.* **57** (2012) 1797.

[6] L.H.C. Braga et al., *An* 8×16*-pixel 92k SPAD time-resolved sensor with on-pixel 64ps 12b TDC and 100MS/s real-time energy histogramming in 0.13* μ*m CIS technology for PET/MRI applications*, in the *IEEE International Solid-State Circuits Conference (ISSCC)*, February 17–21, San Francisco, U.S.A. (2013).

[7] R.J. Walker et al., *A 92k SPAD time-resolved sensor in 0.13* μ*m CIS technology for PET/MRI application*, in the *International Image Sensor Workshop*, June 12–16,, Utah, U.S.A. (2013).

[8] M.W. Fishburn and E. Charbon, *System trade-offs in gamma-ray detection utilizing SPAD arrays and scintillators*, *IEEE Trans. Nucl. Sci.* **57** (2010) 2549.

[9] H.T. van Dam et al., *Improved nearest neighbor methods for gamma photon interaction position determination in monolithic scintillator PET detectors*, *IEEE Trans. Nucl. Sci.* **58** (2011) 2139.

[10] R.J. Walker et al., *High fill factor digital silicon photomultiplier structures in 130 nm CMOS imaging technology*, *IEEE Nucl. Sci. Symp. Med. Imag. Conf.* (2012) 1082.

[11] L.H.C Braga, L. Pancheri, L. Gasparini, M. Perenzoni, R. Walker, R.K. Henderson and D. Stoppa, *A CMOS mini-SiPM detector with in-pixel data compression for PET applications*, *IEEE Nucl. Sci. Symp. Conf. Rec.* (2012) 548.

2013 JINST 8 C12026